Deconfinement of Majorana Vortex Modes Produces a Superconducting Landau Level

M. J. Pacholski,[1] G. Lemut,[1] O. Ovdat,[1] İ. Adagideli,[2,3] and C. W. J. Beenakker[1]
[1]Instituut-Lorentz, Universiteit Leiden, P.O. Box 9506, 2300 RA Leiden, Netherlands
[2]Faculty of Engineering and Natural Sciences, Sabanci University, 34956 Orhanli-Tuzla, Istanbul, Turkey
[3]MESA+ Institute for Nanotechnology, University of Twente, 7500 AE Enschede, Netherlands

(Received 21 January 2021; accepted 26 April 2021; published 2 June 2021)

A spatially oscillating pair potential $\Delta(\boldsymbol{r}) = \Delta_0 e^{2i\boldsymbol{K}\cdot\boldsymbol{r}}$ with momentum $K > \Delta_0/\hbar v$ drives a deconfinement transition of the Majorana bound states in the vortex cores of a Fu-Kane heterostructure (a 3D topological insulator with Fermi velocity v, on a superconducting substrate with gap Δ_0, in a perpendicular magnetic field). In the deconfined phase at zero chemical potential the Majorana fermions form a dispersionless Landau level, protected by chiral symmetry against broadening due to vortex scattering. The coherent superposition of electrons and holes in the Majorana Landau level is detectable as a local density of states oscillation with wave vector $\sqrt{K^2 - (\Delta_0/\hbar v)^2}$. The striped pattern also provides a means to measure the chirality of the Majorana fermions.

DOI: 10.1103/PhysRevLett.126.226801

Introduction.—Deconfinement transitions in physics refer to transitions into a phase where particles can exist as delocalized states, rather than only as bound states. Unlike thermodynamic phase transitions, the deconfinement transition is not associated with a spontaneously broken symmetry but with a change in the momentum space topology of the ground state [1]. A prominent example in superconductors is the appearance of a Fermi surface for Bogoliubov quasiparticles when a superconductor becomes gapless [2–5]. Such a Bogoliubov Fermi surface was observed recently [6].

Motivated by these developments we consider here the deconfinement transition for Majorana zero modes in the vortex core of a topological superconductor. We will demonstrate, analytically and by numerical simulations, that the delocalized phase at zero chemical potential remains a highly degenerate zero-energy level—a superconducting counterpart of the Majorana Landau level in a Kitaev spin liquid [7,8]. Unlike a conventional electronic Landau level, the Majorana Landau level has a nonuniform density profile: quantum interference of the electron and hole components creates spatial oscillations with a wave vector set by the Cooper pair momentum that drives the deconfinement transition.

The system of Ref. [6] is shown in Fig. 1. It is a thin layer of topological insulator deposited on a bulk superconductor, such that the proximity effect induces a pairing gap Δ_0 in the surface states. A superflow with Cooper pair momentum $\boldsymbol{K}$ lowers the excitation energy for quasiparticles with velocity $\boldsymbol{v}$ by the Doppler shift $\boldsymbol{v}\cdot\boldsymbol{K}$, closing the gap when vK exceeds Δ_0. Following Fu and Kane [9], we add a perpendicular magnetic field B to confine a Majorana zero mode to the core of each $h/2e$ vortex that penetrates the superconductor. We seek to characterize the deconfined phase that emerges when $vK > \Delta_0$.

Confined phase.—To set the stage we first investigate the confined phase for $vK < \Delta_0$. Electrons on the two-dimensional (2D) surface of a 3D topological insulator have the Dirac Hamiltonian $v\boldsymbol{k}\cdot\boldsymbol{\sigma} - \mu$, with μ the chemical potential, v the energy-independent Fermi velocity, $\boldsymbol{k} = (k_x, k_y)$ the momentum operator in the $x-y$ surface plane, and $\boldsymbol{\sigma} = (\sigma_x, \sigma_y)$ two Pauli spin matrices. (The 2×2 unit matrix σ_0 is implicit when the Hamiltonian contains a scalar term.) Application of a perpendicular magnetic field B (in the z direction), adds an in-plane vector potential $\boldsymbol{A} = (A_x, A_y)$ to the momentum, $\boldsymbol{k} \mapsto \boldsymbol{k} - e\boldsymbol{A}$. The electron charge is $+e$, and for ease of notation we will set v and $\hbar$ both equal to unity in most equations.

The superconducting substrate induces a pair potential $\Delta = \Delta_0 e^{i\phi}$. The phase field $\phi(\boldsymbol{r})$ winds by $\pm 2\pi$ around each vortex, at position $\boldsymbol{R}_n$, as expressed by

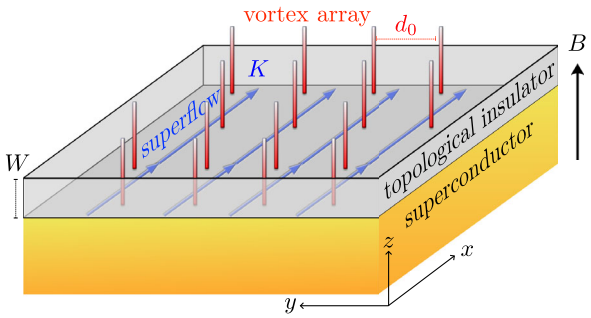

FIG. 1. Schematic of the Fu-Kane heterostructure [9], a topological insulator with induced superconductivity (gap Δ_0) in a perpendicular magnetic field B. Vortices (red) bind midgap states known as Majorana zero modes. Here we study the deconfinement transition in response to an in-plane supercurrent (blue arrows, momentum K). When $vK > \Delta_0$ the zero modes delocalize into a Majorana Landau level.

$$\nabla \times \nabla\phi(\boldsymbol{r}) = \pm 2\pi\hat{z}\sum_n \delta(\boldsymbol{r}-\boldsymbol{R}_n), \qquad \nabla^2\phi = 0. \quad (1)$$

The pair potential couples electrons and holes in the 4×4 Bogoliubov–de Gennes (BdG) Hamiltonian

$$H = \begin{pmatrix} K\sigma_x + (\boldsymbol{k}-e\boldsymbol{A})\cdot\boldsymbol{\sigma} & \Delta_0 e^{i\phi} \\ \Delta_0 e^{-i\phi} & K\sigma_x - (\boldsymbol{k}+e\boldsymbol{A})\cdot\boldsymbol{\sigma} \end{pmatrix}, \quad (2)$$

at zero chemical potential, including a superflow momentum field $K \geq 0$ in the x direction [10]. The superflow can be a screening current in response to a magnetic field in the y direction [6], or it can result from an externally imposed flux bias or current bias. The Zeeman energy from an in-plane magnetic field has an equivalent effect [3] (although it was estimated to be negligible relative to the orbital effect of the field in the experiment [6]).

For $vK < \Delta_0$ a pair of Majorana zero modes will appear in each vortex core, one at the top surface and one at the bottom surface. We consider these separately [11,12]. Setting $\Delta(\boldsymbol{r}) = \Delta_0(r)e^{\pm i\theta}$, in polar coordinates (r,θ) for a $\pm 2\pi$ phase vortex at the origin, we need to solve the zero-mode equation $H_\pm \Psi_\pm = 0$ with

$$H_\pm = \begin{pmatrix} K\sigma_x - (i\nabla + e\boldsymbol{A})\cdot\boldsymbol{\sigma} & \Delta_0(r)e^{\pm i\theta} \\ \Delta_0(r)e^{\mp i\theta} & K\sigma_x + (i\nabla - e\boldsymbol{A})\cdot\boldsymbol{\sigma} \end{pmatrix}. \quad (3)$$

The pair potential amplitude $\Delta_0(r)$ increases from 0 at $r=0$ to a value $\Delta_0 > 0$ when r becomes larger than the superconducting coherence length $\xi_0 = \hbar v/\Delta_0$.

When $K = 0$ this is a familiar calculation [13] which is readily generalized to $K > 0$. The Majorana zero mode has a definite chirality $\mathcal{C}$, meaning that its four-component wave function $\Psi_\pm$ is an eigenstate of the chirality operator $\Lambda = \mathrm{diag}(1,-1,-1,1)$ with eigenvalue $\mathcal{C} = \pm 1$. One has $\Psi_+ = (i\psi_+, 0, 0, \psi_+)$, $\Psi_- = (0, i\psi_-, \psi_-, 0)$ with [14]

$$\psi_\pm(\boldsymbol{r}) = e^{\mp Ky} e^{\mp\chi(\boldsymbol{r})} \exp\left(-\int_0^r \Delta_0(r')dr'\right), \quad (4a)$$

$$\chi(\boldsymbol{r}) = \frac{e}{2\pi}\int d\boldsymbol{r}' B(\boldsymbol{r}') \ln|\boldsymbol{r}-\boldsymbol{r}'|. \quad (4b)$$

The factor $e^{\mp\chi(\boldsymbol{r})}$ is a power law for large r, so the zero mode is confined exponentially to the vortex core as long as $K < \Delta_0$. When $K > \Delta_0$ the solution (4) is no longer normalizable: it diverges exponentially along the y axis. This signals a transition into a deconfined phase, which we consider next.

Deconfined phase.—In Fig. 2 we show results from a numerical simulation of the deconfinement transition for the model Hamiltonian described below. The left panel shows zero modes confined to a pair of vortex cores for $K < \Delta_0$; the right panel shows the deconfined state for

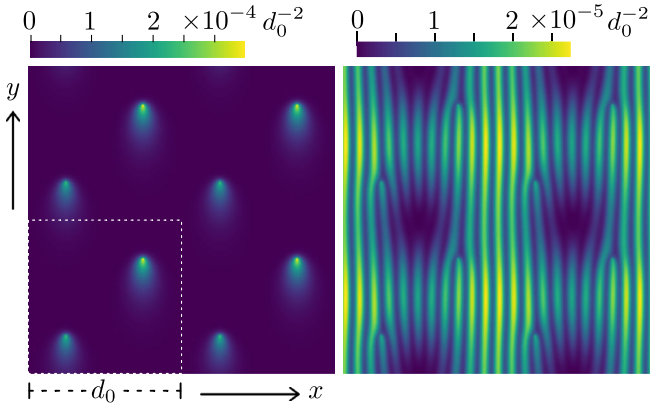

FIG. 2. Intensity profile $|\Psi(x,y)|^2$ of a Majorana zero mode in the vortex lattice [16]. Left panel: confined phase ($K < \Delta_0$). Right panel: deconfined phase ($K > \Delta_0$). The dotted square indicates the unit cell containing a pair of $h/2e$ vortices. These plots are for Majorana fermions of positive chirality; for negative chirality the density profile is inverted, $y \mapsto -y$.

$K > \Delta_0$. The decay $|\Psi| \propto e^{-Ky}e^{-\Delta_0 r}$ in the confined phase is anisotropic, with a decay rate Δ_0 along the x axis and two different decay rates $\Delta_0 \pm K$ in the $\pm y$ direction. The direction into which the zero mode decays more slowly is set by the chirality [15]: Fig. 2 shows $\mathcal{C} = +1$ with a slow decay in the $-y$ direction, and for $\mathcal{C} = -1$ the slow decay is in the $+y$ direction.

In the deconfined phase the zero-mode density profile has a pronounced periodic modulation in the x direction, parallel to the superflow, with bifuration points at the vortex cores. This striped pattern is unexpected for a Landau level. We present an analytical description.

Chiral symmetry protected Majorana Landau level.—The chiral symmetry of the Hamiltonian (2) plays a key role in our analysis of the Majorana Landau level, similar to the role it plays for Landau level quantization in graphene [17,18] and in a Weyl superconductor [19]. Chiral symmetry means that H at $\mu = 0$ anticommutes with Λ. The Hamiltonian then becomes block off diagonal in the basis of eigenstates of Λ,

$$U^\dagger H U = \begin{pmatrix} 0 & \Xi \\ \Xi^\dagger & 0 \end{pmatrix}, \qquad U = \begin{pmatrix} 1 & 0 & 0 & 0 \\ 0 & 0 & 1 & 0 \\ 0 & 0 & 0 & 1 \\ 0 & 1 & 0 & 0 \end{pmatrix}, \quad (5a)$$

$$\Xi = \begin{pmatrix} k_- - eA_- + K & \Delta_0 e^{i\phi} \\ \Delta_0 e^{-i\phi} & -k_+ - eA_+ + K \end{pmatrix}, \quad (5b)$$

where we have abbreviated $k_\pm = k_x \pm ik_y$, $A_\pm = A_x \pm iA_y$.

A zero mode is either a wave function $(u,0)$ of positive chirality with $\Xi^\dagger u = 0$ or a wave function $(0,u)$ of negative chirality with $\Xi u = 0$. The difference between the number of normalizable eigenstates of either chirality is called the

index of the Hamiltonian. It is topologically protected, meaning it is insensitive to perturbations [20].

Vortices are strong scatterers [21], completely obscuring the Landau level quantization in a nontopological superconductor [22]. Here chiral symmetry ensures that the vortices cannot broaden the zeroth Landau level.

Helmholtz equation for the Majorana Landau level.—Let us focus on the Landau level of positive chirality, described by the equation $\Xi^\dagger u = 0$. This 2×2 matrix differential equation can be simplified by the substitution

$$u(\boldsymbol{r}) = e^{-Ky-q(\boldsymbol{r})} e^{(1/2)i\phi(\boldsymbol{r})\sigma_z} \tilde{u}(\boldsymbol{r}), \tag{6}$$

$$\text{with} \quad \partial_x q = -\frac{1}{2}\partial_y \phi + eA_y, \qquad \partial_y q = \frac{1}{2}\partial_x \phi - eA_x, \tag{7}$$

$$\Rightarrow \begin{pmatrix} -i\partial_x + \partial_y & \Delta_0 \\ \Delta_0 & i\partial_x + \partial_y \end{pmatrix} \tilde{u} = 0. \tag{8}$$

The fields $\boldsymbol{A}$, ϕ, and K no longer appear explicitly in the differential equation (8) for $\tilde{u}$, but they still determine the solution by the requirements of normalizability and single valuedness of the zero mode u.

Outside of the vortex core the spatial dependence of the pair potential amplitude Δ_0 may be neglected, and one further simplification is possible: Substitution of $\tilde{u} = (f, g)$ gives $g = \Delta_0^{-1}(i\partial_x - \partial_y) f$ and a scalar second-order differential equation for f,

$$\nabla^2 f = \Delta_0^2 f. \tag{9}$$

In the context of classical wave equations this is the Helmholtz equation with an imaginary wave vector.

Equation (6) requires that $\tilde{u}$ and hence f have an exponential envelope e^{Ky} in the y direction. The Helmholtz equation (9) then ties that to a plane wave $\propto e^{\pm iQx}$ in the x direction, with wave vector $Q = \sqrt{K^2 - \Delta_0^2}$. This already explains the striped pattern in the numerical simulations of Fig. 2. For a more detailed comparison we proceed to a full solution of the Helmholtz equation.

Analytical solution of the Majorana Landau level wave function.—The solutions of Eq. (9) for f are constrained by the requirements of normalizability and single valuedness of u. To determine the normalizability constraint we give the field $q(\boldsymbol{r})$ defined in Eq. (7) the integral representation [23]

$$q(\boldsymbol{r}) = \frac{1}{2\Phi_0}\int d\boldsymbol{r}' B(\boldsymbol{r}') \ln|\boldsymbol{r} - \boldsymbol{r}'| - \frac{1}{2}\sum_n \ln|\boldsymbol{r} - \boldsymbol{R}_n|. \tag{10}$$

We consider $\mathcal{N}$ vortices (each of $+2\pi$ vorticity) in a region S enclosing a flux $\Phi = N\Phi_0$, with $\Phi_0 = h/2e$ the superconducting flux quantum [24]. If we set $B \to 0$ outside of S, the field $q(\boldsymbol{r}) \to (1/2)(\Phi/\Phi_0 - \mathcal{N}) \ln r = 0$ for $r \to \infty$. In view of Eq. (6), normalizability requires that $e^{-Ky} f$ is square integrable for $r \to \infty$. Near a vortex core $e^{-q} f \propto |\boldsymbol{r} - \boldsymbol{R}_n|^{1/2} f$ must be square integrable [25].

Concerning the single valuedness, the factor $e^{i\phi/2}$ in Eq. (6) introduces a branch cut at each vortex position $\boldsymbol{R}_n$, across which the function f should change sign, to ensure a single-valued u. This is a local constraint: branch cuts can be connected pairwise; hence there is no sign change in f on a contour encircling a vortex pair.

We have obtained an exact analytical solution [26] of the Helmholtz equation in the limit in which the separation of a vortex pair goes to zero. We place the two vortices at the origin of a disk of radius R, enclosing a flux h/e, with zero magnetic field outside of the disk. The envelope function then equals $e^{-q(r)} = r_{\min} e^{-r_{\min}^2/2R^2}$, with $r_{\min} = \min(r, R)$.

The two independent solutions are given by $\tilde{u} = (f_1, f_0)$ and $\tilde{u}' = \sigma_x \tilde{u}^*$, with

$$f_n = 2i^n e^{-in\theta} \mathrm{K}_n(\Delta_0 r) - \int_{-Q}^{Q} dp C_n(p) e^{ixp + y\sqrt{\Delta_0^2 + p^2}},$$
$$C_n(p) = \Delta_0^{-n} (\Delta_0^2 + p^2)^{-1/2} (p - \sqrt{\Delta_0^2 + p^2})^n. \tag{11}$$

The vortex pair is at the origin, with $x + iy = re^{i\theta}$, and K_n is a Bessel function.

The corresponding zero modes follow from Eq. (6),

$$u = e^{-q(r)} e^{-Ky} (e^{i\theta} f_1, e^{-i\theta} f_0), \qquad u' = \sigma_x u^*. \tag{12}$$

For small r the zero modes tend to a constant (the factor $1/r$ from K_1 is canceled by the factor r from e^{-q}). The large-r asymptotics follows upon an expansion of the integrand around the extremal points $\pm Q$, giving

$$f_n \to (-1)^n \frac{e^{Ky}}{\Delta_0^n} \left(\frac{(K+Q)^n e^{-iQx}}{iKx - Qy} - \frac{(K-Q)^n e^{iQx}}{iKx + Qy} \right). \tag{13}$$

The zero modes decay as $e^{-Ky} f_n \propto 1/r$ for $r \gg R$, which needs to be regularized for a square-integrable wave function [27–29]. In a chain of vortices (spacing b), the superposition of the solution (13) decays exponentially in the direction perpendicular to the chain [26]. The decay length is $\lambda = bK/Q$ or $\lambda = bQ/K$ for a chain oriented along the x or y axis, respectively.

Numerical simulation.—For a numerical study of the deconfinement transition we represent the topological insulator layer by the low-energy Hamiltonian [30,31]

$$H_0(\boldsymbol{k}) = (v/a_0) \sum_{j=x,y} \sigma_j \sin k_j a_0 + \sigma_z M(k) - \mu,$$
$$M(k) = M_0 - (M_1/a_0^2) \sum_{j=x,y} (1 - \cos k_j a_0), \tag{14}$$

in the basis $\Psi = 2^{-1/2}(\psi_{\uparrow\text{upper}} + \psi_{\uparrow\text{lower}}, \psi_{\downarrow\text{upper}} - \psi_{\downarrow\text{lower}})$ of spin-up and spin-down states on the upper and lower surfaces [32]. The atomic lattice constant is a_0, the Fermi

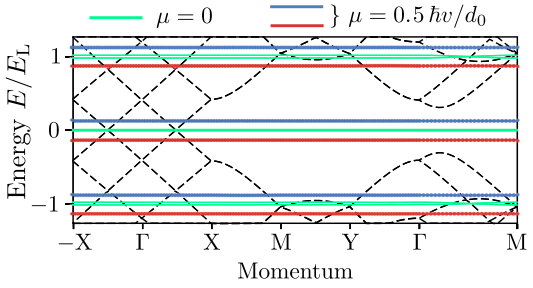

FIG. 3. Dispersion relation of the topological superconductor, calculated from the model Hamiltonian (14) for zero magnetic field (black dashed lines, chemical potential $\mu = 0$) and in the presence of the magnetic vortex lattice (colored flatbands at charge $\pm q_{\rm eff} e$ for two values of μ). For both datasets $K = 2\Delta_0 = 20\hbar v/d_0$.

velocity is v, and the chemical potential is μ. Hybridization of the states on the two surfaces introduces the mass term $M(k)$. We set $M_0 = 0$ to avoid the opening of a gap at $k = 0$ [11] but retain a nonzero $M_1 = 0.2a_0 v$ in order to eliminate the fermion doubling at $a_0\boldsymbol{k} = (\pi, \pi)$.

In the corresponding BdG Hamiltonian the electron block $H_0(\boldsymbol{k} - e\boldsymbol{A} + \boldsymbol{K})$ is coupled to the hole block $-H_0(\boldsymbol{k} + e\boldsymbol{A} - \boldsymbol{K})$ by the s-wave pair potential $\Delta_0 e^{i\phi}$, which we take to be the same for both layers. We assume a strong type-II superconductor, for which we can take a uniform magnetic field B and uniform pair potential amplitude Δ_0. The $+2\pi$ vortices are positioned on a square lattice (lattice constant $d_0 = 302a_0$) with two vortices per unit cell.

The spectrum is calculated using the KWANT tight-binding code [33,34]. In Fig. 3 we show the dispersionless Landau levels for both chemical potential $\mu = 0$ and for nonzero μ. The zeroth Landau level has energy $E_0 = \pm q_{\rm eff}\mu$, with $q_{\rm eff} e$ the charge expectation value.

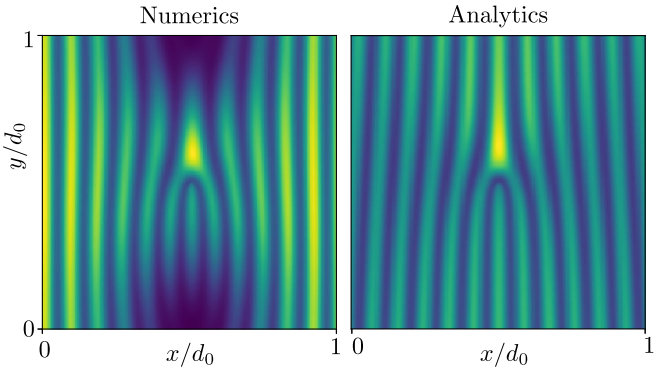

FIG. 4. Left panel: numerically calculated intensity profile $|\Psi(x, y)|^2$ of the zeroth Landau level in a vortex lattice with a pair of $h/2e$ vortices at the center of the unit cell ($K = 2\Delta_0 = 40\hbar v/d_0$, $\mu = 0$). Right panel: analytical result from the solution of the Helmholtz equation (9) for a single h/e vortex [37].

For the model Hamiltonian (2) we have [35] $q_{\rm eff} = Q/K = \sqrt{1 - \Delta_0^2/K^2}$. The numerics at $K = 2\Delta_0$ give a value 0.85, which is within 2% of $\sqrt{3/4} = 0.866$. The first Landau level is expected at energy $E_1 = E_L \pm q_{\rm eff}\mu$ with $E_L = \sqrt{4\pi q_{\rm eff}}\hbar v/d_0$, again in very good agreement with the numerics. Notice that the flatness of the dispersion persists at nonzero μ, even though the topological protection due to chiral symmetry [36] is only rigorously effective at $\mu = 0$.

In Fig. 4 we compare the numerical and analytical results for the case in which the two $h/2e$ vortices are both placed at the center of the unit cell. The agreement is quite satisfactory, given the different geometries (a vortex lattice in the numerics, a single h/e vortex in the analytics).

Striped local density of states.—The striped pattern of the Majorana Landau level is observable by tunneling spectroscopy, which measures the local density of states

$$\rho(\boldsymbol{r}) = \sum_{\boldsymbol{k}} [|\psi_e(\boldsymbol{r})|^2 f'(E_0 - eV) + |\psi_h(\boldsymbol{r})|^2 f'(E_0 + eV)], \tag{15}$$

averaged over the 2D magnetic Brillouin zone, $\sum_{\boldsymbol{k}} = (2\pi)^{-2} \int dk_x dk_y$, weighted by the derivative of the Fermi function. If E_0 is much larger than the temperature, the sign of the bias voltage V determines whether the electron component ψ_e or the hole component ψ_h contributes, so these can be measured separately.

As shown in Fig. 5, the oscillations are most pronounced for the hole component when $\mu > 0$ (or, equivalently, the electron component when $\mu < 0$). This asymmetry in the tunneling current for $V = \pm E_0$ is an additional experimental signature of the effect.

Conclusion.—Concerning the experimental feasibility, we note that the gap closing due to a superflow has already been observed [6], and Majorana vortex lattices in a perpendicular field of 250 mT have been detected by scanning probes in several experiments [38]—so by

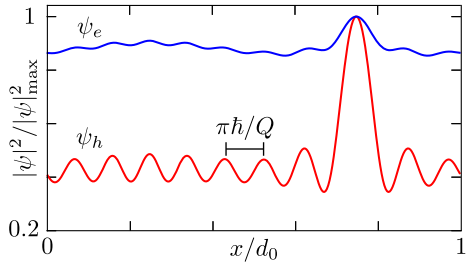

FIG. 5. Electron and hole contributions to the local density of states in the zeroth Landau level along a line parallel to the x axis which passes close to a vortex core at $x = y = 3d_0/4$. The curves are plots of $\sum_{\boldsymbol{k}} |\psi_{e,h}(x, y)|^2$ normalized to unit peak height at the vortex core. The parameters are $K = 2\Delta_0 = 40\hbar v/d_0$, $\mu = 0.5\hbar v/d_0$. The expected oscillation period of $\pi\hbar/Q = 0.091 d_0$ is indicated.

combining these two ingredients the Majorana Landau level should become accessible. The main additional requirement is for the Fermi level to be sufficiently small, $\mu < \min(E_L, \Delta_0) \simeq 1$ meV at 250 mT, to benefit from the protection afforded by chiral symmetry. Experiments [39] where μ was tuned through the charge neutrality point give confidence that this is feasible.

The striped interference pattern in the local density of states, with wave number $Q = \sqrt{K^2 - (\Delta_0/\hbar v)^2}$ ($\simeq 2\pi/0.2$ μm for $K = 2\Delta_0/\hbar v$ at typical values of $\Delta_0 =$ 1 meV and $v = 10^5$ m/s) should be accessible by scanning probe spectroscopy. Surface defects would themselves introduce Friedel oscillations in the density of states, but the highly directional pattern that is the hallmark of the Majorana Landau level would stand out.

The Majorana Landau level provides a realization of a flatband with extended wave functions, in which interaction effects are expected to be enhanced due to the quenching of kinetic energy. Interacting Majorana fermions in a Fu-Kane superconductor have been studied by placing vortices in close proximity inside a quantum dot [40]. The deconfinement transition provides a means to open up the system and obtain a fully 2D flatband with widely separated vortices. An intriguing topic for further research would be to investigate how the exchange of vortices operates on this highly degenerate manifold.

We have benefited from discussions with A. R. Akhmerov and A. Donis Vela. This project has received funding from the Netherlands Organization for Scientific Research (NWO/OCW) and from the European Research Council (ERC) under the European Union's Horizon 2020 research and innovation program.

[1] G. E. Volovik, Quantum phase transitions from topology in momentum space, Lect. Notes Phys. **718**, 31 (2007).
[2] D. F. Agterberg, P. M. R. Brydon, and C. Timm, Bogoliubov Fermi Surfaces in Superconductors with Broken Time-Reversal Symmetry, Phys. Rev. Lett. **118**, 127001 (2017).
[3] N. F. Q. Yuan and L. Fu, Zeeman-induced gapless superconductivity with a partial Fermi surface, Phys. Rev. B **97**, 115139 (2018).
[4] S. Autti, J. T. Mäkinen, J. Rysti, G. E. Volovik, V. V. Zavjalov, and V. B. Eltsov, Exceeding the Landau speed limit with topological Bogoliubov Fermi surfaces, Phys. Rev. Research **2**, 033013 (2020).
[5] J. M. Link and I. F. Herbut, Bogoliubov-Fermi Surfaces in Noncentrosymmetric Multicomponent Superconductors, Phys. Rev. Lett. **125**, 237004 (2020).
[6] Z. Zhu, M. Papaj, X.-A. Nie, H.-K. Xu, Y.-S. Gu, X. Yang, D. Guan, S. Wang, Y. Li, C. Liu, J. Luo, Z.-A. Xu, H. Zheng, L. Fu, and J.-F. Jia, Discovery of segmented Fermi surface induced by Cooper pair momentum, arXiv:2010.02216. For a commentary on this experiment, see https://doi.org/10.36471JCCM_October_2020_01.
[7] S. Rachel, L. Fritz, and M. Vojta, Landau levels of Majorana Fermions in a spin liquid, Phys. Rev. Lett. **116**, 167201 (2016).
[8] B. Perreault, S. Rachel, F. J. Burnell, and J. Knolle, Majorana Landau-level Raman spectroscopy, Phys. Rev. B **95**, 184429 (2017).
[9] L. Fu and C. L. Kane, Superconducting Proximity Effect and Majorana Fermions at the Surface of a Topological Insulator, Phys. Rev. Lett. **100**, 096407 (2008).
[10] The term $K\sigma_x$ in the BdG Hamiltonian (2) is equivalent, upon a gauge transformation, to a gradient $2Kx$ in ϕ.
[11] The overlap of states on the top and bottom surfaces of the topological insulator thin film shifts the Majorana Landau away from $E = 0$ by the hybridization gap while keeping the spatial structure of the wave functions intact. We include this effect in the calculations in Appendix A of the Supplemental Material [12].
[12] See Supplemental Material at http://link.aps.org/supplemental/10.1103/PhysRevLett.126.226801 for the details of the calculations.
[13] R. Jackiw and P. Rossi, Zero modes of the vortex-fermion system, Nucl. Phys. **B190**, 681 (1981).
[14] To understand how the solution (4) relates to the $K = 0$ solution in Ref. [13], note the (nonunitary) transformation $e^{Ky\Lambda} H_\pm e^{Ky\Lambda} = H_\pm + K\sigma_x$, with $\Lambda = \mathrm{diag}(1, -1, -1, 1)$. The spinor $\Psi_\pm$ is an eigenstate of Λ with eigenvalue ± 1, so if $H_\pm \Psi_\pm = 0$ for $K = 0$, then $H_\pm e^{\pm Ky} \Psi_\pm = 0$ for $K \neq 0$.
[15] The anisotropic decay of the Majorana zero mode in the left panel of Fig. 2 can be understood as the effect of the Magnus force which the superflow momentum $\boldsymbol{K} = K\hat{x}$ exerts on the axial spin $\boldsymbol{S} = \mathcal{C}\hat{z}$ of the Majorana fermions (as determined by their chirality $\mathcal{C} = \pm 1$). The direction of slow decay of the zero mode is given by the cross product $\boldsymbol{K} \times \boldsymbol{S}$.
[16] The data in Fig. 2 are obtained from the tight-binding Hamiltonian (14) of the topological insulator layer. The parameters are $\Delta_0 = 20\hbar v/d_0$, $d_0 = 302a_0$, $B = h/ed_0^2$, $\mu = 0$, $M_0 = 0$, and $M_1 = 0.2a_0$. The vortex pair in a unit cell is at the positions $(x, y) = (d_0/4)(1, 1)$ and $(d_0/4)(3, 3)$. The superflow momentum K equals $0.8\Delta_0/v$ in the left panel and $2\Delta_0/v$ in the right panel.
[17] M. I. Katsnelson and M. F. Prokhorova, Zero-energy states in corrugated bilayer graphene, Phys. Rev. B **77**, 205424 (2008).
[18] J. Kailasvuori, Pedestrian index theorem à la Aharonov-Casher for bulk threshold modes in corrugated multilayer graphene, Europhys. Lett. **87**, 47008 (2009).
[19] M. J. Pacholski, C. W. J. Beenakker, and I. Adagideli, Topologically Protected Landau Level in the Vortex Lattice of a Weyl Superconductor, Phys. Rev. Lett. **121**, 037701 (2018).
[20] Y. Aharonov and A. Casher, Ground state of a spin-1/2 charged particle in a two-dimensional magnetic field, Phys. Rev. A **19**, 2461 (1979).
[21] A. S. Mel'nikov, Quantization of the quasiparticle spectrum in the mixed state of d-wave superconductors, J. Phys. Condens. Matter **11**, 4219 (1999).
[22] M. Franz and Z. Tešanović, Quasiparticles in the Vortex Lattice of Unconventional Superconductors: Bloch Waves or Landau Levels?, Phys. Rev. Lett. **84**, 554 (2000).
[23] The integral equation (10) for $q(\boldsymbol{r})$ follows from the definition (7), which implies that $\nabla^2 q(\boldsymbol{r}) = \hat{z} \cdot \nabla \times [e\boldsymbol{A} - (1/2)\nabla\phi] = eB - \pi \sum_n \delta(\boldsymbol{r} - \boldsymbol{R}_n)$. The Green's function of this 2D

Poisson equation is $(2\pi)^{-1}\ln|\boldsymbol{r}-\boldsymbol{r}'|$. Also note that $\Phi_0 \equiv \pi/e$ in units where $\hbar \equiv 1$.

[24] We assume there is an even number of vortices in S. If the number of vortices is odd, a zero-energy edge state along the perimeter of S will ensure that the total number of Majorana zero modes remains even.

[25] This normalization requirement at the vortex core ties the chirality of the Majorana zero modes to the sign of the vorticity. If we would have chosen -2π vortices the field $q(\boldsymbol{r})$ would tend to $+(1/2)\ln|r-\boldsymbol{R}_n|$ near a vortex core, and the product $e^{-q}f \propto |\boldsymbol{r}-\boldsymbol{R}_n|^{-1/2}f$ would not have been square integrable.

[26] Details of the solution of the Helmholtz equation are given in Appendixes B and C of the Supplemental Material [40].

[27] The $1/r$ decay of the deconfined Majorana zero mode implies a density of states peak which decays slowly $\propto 1/\ln L$ as a function of the system size L. There is a formal similarity here with the zero modes originating from vacancies in a 2D bipartite lattice [28,29].

[28] B. Sutherland, Localization of electronic wave functions due to local topology, Phys. Rev. B **34**, 5208 (1986).

[29] V. M. Pereira, F. Guinea, J. M. B. Lopes dos Santos, N. M. R. Peres, and A. H. Castro Neto, Disorder Induced Localized States in Graphene, Phys. Rev. Lett. **96**, 036801 (2006).

[30] W.-Y. Shan, H.-Z. Lu, and S.-Q. Shen, Effective continuous model for surface states and thin films of three-dimensional topological insulators, New J. Phys. **12**, 043048 (2010).

[31] S.-B. Zhang, H.-Z. Lu, and S.-Q. Shen, Edge states and integer quantum Hall effect in topological insulator thin films, Sci. Rep. **5**, 13277 (2015).

[32] In the basis $\Psi = (\psi_{\uparrow\text{upper}}, \psi_{\downarrow\text{upper}}, \psi_{\uparrow\text{lower}}, \psi_{\downarrow\text{lower}})$ the 4×4 Hamiltonian of the topological insulator layer is $H_0 = t_0 \sum_{j=x,y} \tau_z \sigma_j \sin k_j a_0 + \tau_x \sigma_0 M(k) - \mu$, with Pauli matrix τ_z acting on the layer index. A unitary transformation block diagonalizes the Hamiltonian. One of the 2×2 blocks is given in Eq. (14); the other block has M replaced by $-M$.

[33] C. W. Groth, M. Wimmer, A. R. Akhmerov, and X. Waintal, KWANT: A software package for quantum transport, New J. Phys. **16**, 063065 (2014).

[34] Details of the method of numerical simulation, with supporting data, are given in Appendix A of the Supplemental Material [40].

[35] The renormalized charge q_{eff} in the Majorana Landau level is calculated in Appendix D of the Supplemental Material [12]. That calculation also gives the renormalized Fermi velocity $v_{\text{eff}} = \sqrt{v_x v_y} = \sqrt{q_{\text{eff}}}\, v$ that appears in the Landau level energy E_L.

[36] The chiral symmetry at $\mu = 0$ is broken by the mass term $M(k)$ in the Hamiltonian (14). This residual chiral symmetry breaking is visible in Fig. 3 as a very small splitting of the $\mu = 0$ Landau levels (green flatbands).

[37] The comparison between numerics and analytics in Fig. 4 involves no adjustable parameters. To compare the same state in the degenerate zeroth Landau level we choose the state with left-right reflection symmetry. There are two of these, the other is compared in Appendix E of the Supplemental Material [12].

[38] H.-H. Sun and J.-F. Jia, Detection of Majorana zero mode in the vortex, npj Quantum Mater. **2**, 34 (2017).

[39] S. Cho, B. Dellabetta, A. Yang, J. Schneeloch, Z. Xu, T. Valla, G. Gu, M. J. Gilbert, and N. Mason, Symmetry protected Josephson supercurrents in three-dimensional topological insulators, Nat. Commun. **4**, 1689 (2013).

[40] D. I. Pikulin and M. Franz, Black Hole on a Chip: Proposal for a Physical Realization of the SYK Model in a Solid-State System, Phys. Rev. X **7**, 031006 (2017).